Synthetically Encoded Ultrashort-Channel Nanowire Transistors for Fast, Pointlike Cellular Signal Detection

Share Your Story

The Harvard community has made this article openly available.
Please share how this access benefits you. Submit a story .

Accessibility

Synthetically-encoded ultrashort-channel nanowire transistors for fast, point-like cellular signal detection

Tzahi Cohen-Karni[1,†], Didier Casanova [1,‡], James F. Cahoon[‡], Quan Qing[‡], David C. Bell[†, #], Charles M. Lieber*[†,‡]

[†]School of Engineering and Applied Science, Harvard University, Cambridge, Massachusetts 02138

[‡]Department of Chemistry and Chemical Biology, Harvard University, Cambridge, Massachusetts 02138

[#]Center for Nanoscale Systems, Harvard University, Cambridge, Massachusetts 02138

[1]These authors contributed equally to this work

*Corresponding authors: Email: cml@cmliris.harvard.edu

Abstract. Nanostructures, which have sizes comparable to biological functional units involved in cellular communication, offer the potential for enhanced sensitivity and spatial resolution compared to planar metal and semiconductor structures. Silicon nanowire (SiNW) field-effect transistors (FETs) have been used as a platform for biomolecular sensors, which maintain excellent signal-to-noise ratios while operating on lengths scales that enable efficient extra- and intra-cellular integration with living cells. Although the NWs are tens of nanometers in diameter, the active region of the NW FET devices typically spans microns, limiting both the length and time scales of detection achievable with these nanodevices. Here, we report a new synthetic method that combines gold-nanocluster catalyzed vapor-

liquid-solid (VLS) and vapor-solid-solid (VSS) NW growth modes to produce synthetically encoded NW devices with ultrasharp (<5 nm) n-type highly-doped (n^{++}) to lightly-doped (n) transitions along the NW growth direction, where n^{++} regions serve as source/drain (S/D) electrodes and the n-region functions as an active FET channel. Using this method, we synthesized short-channel $n^{++}/n/n^{++}$ SiNW FET devices with independently controllable diameters and channel lengths. SiNW devices with channel lengths of 50, 80, and 150 nm interfaced with spontaneously beating cardiomyocytes exhibited well-defined extracellular field potential signals with signal-to-noise values of ca. 4 independent of device size. Significantly, these "point-like" devices yield peak-widths of ~500 µs, which is comparable to the reported time constant for individual sodium ion channels. Multiple FET devices with device separations smaller than 2 µm were also encoded on single SiNWs, thus enabling multiplexed recording from single cells and cell networks with device-to-device time resolution on the order of a few microseconds. These short-channel SiNW FET devices provide a new opportunity to create nanoscale biomolecular sensors that operate on the length and time scales previously inaccessible by other techniques but necessary to investigate fundamental, sub-cellular biological processes.

NWs have been exploited for ultrasensitive detection of biological markers,[1-2] single virus particles,[3] and for electrical recording from cells,[4-7] and tissue.[10, 11] Electrical signal recording with nanostructures, such as SiNWs, has several advantages compared to conventional detection techniques with planar field effect transistors (FETs) and multielectrodes arrays (MEAs).[12-16] First, SiNW devices have been shown to exhibit high sensitivity with signal-to-noise that outperforms planar structures.[4-6] Second, the small diameters and controlled structural topology of NWs[17] have enabled the first FET-based intracellular measurements.[8] Third, nanostructures have been shown to enhance cellular adhesion

and activity.[18-25] Last, the diameters of synthesized NWs have dimensions that are close to the macromolecular assemblies within the cell membrane crucial for function and signal transduction.[4-6]

Despite these advances with synthesized NWs for cellular recording, the devices used to date for extracellular measurements are limited in the sense that they are best described as "line-like" detectors since the active detector lengths have been on the order of 1-2 μm.[4-7] Ideally, one would like to develop "point-like" detectors where the active NW detector length is comparable to the NW diameter. Electron beam lithography can be used to fabricate directly sub-100 nm devices, although the fabricated metal electrodes physically-limit cell access and electrostatically-screen the active NW device.[26] Dopant modulation can be used to synthesize directly lightly-doped active channels connected to heavily-doped NW S/D contact arms, although it is difficult to prepare well-defined short-channel devices due to the rapid growth rates during nanocluster-catalyzed VLS growth and the dopant concentration gradients on the order of the nanocluster diameter.

Interestingly, a potential solution to this synthetic conundrum was recently described by Ross and coworkers with the synthesis of atomically-abrupt Si/Ge axial NW heterojunctions.[27, 28] In this work, growth was carried out at temperatures below the catalyst-Si/Ge eutectic point such that the nanocluster catalyst is in the solid versus liquid state, and thus growth is termed VSS. The abrupt Si/Ge heterojunctions along the growth direction of the NWs were made possible due to slow growth rates of the VSS mechanism, which are at least 10-100 times lower than for VLS grown nanowires,[29-31] and the fact that there is not a reactant concentration gradient through the nanocluster catalyst. Here, we exploit this VSS concept to synthesize sub-100 nm NW devices with sharp dopant profiles for the first time and utilize these new "point-like" NW devices to record extracellular action potentials.

Our approach to synthesize SiNWs with controlled NW dopant profiles involves sequential modulation of temperature and the PH_3 dopant reactant concentration as outlined schematically in Figure 1A.[32] First, we synthesize a highly doped n-type (n^{++}) segment that will serve as the S electrode using the nanocluster-catalyzed VLS mechanism at a temperature above the Au-Si eutectic point (T_{eu}). Second, in order to synthesize the short channel we reduce the temperature below T_{eu} to solidify the Au

catalyst and transition to a VSS growth mechanism, where growth rate is ca. 10-100 times slower than growth by VLS. After the transition to VSS the PH_3 reactant is either reduced (marked as "n") or completely stopped (marked as "i") for a set period of time to define the active FET channel, and then the dopant reactant is again increase to begin growth of n^{++} D electrode. Last, we raise the temperature above T_{eu} to transition back to a VLS growth mechanism and complete the growth of this n^{++} electrode. Short channel NWFET devices made in this way can be used to interface to cells at a scale where the active channel size is comparable to the size of a few ion-channels embedded in the membrane of an electrogenic   cell   (Figure   1B).[39]
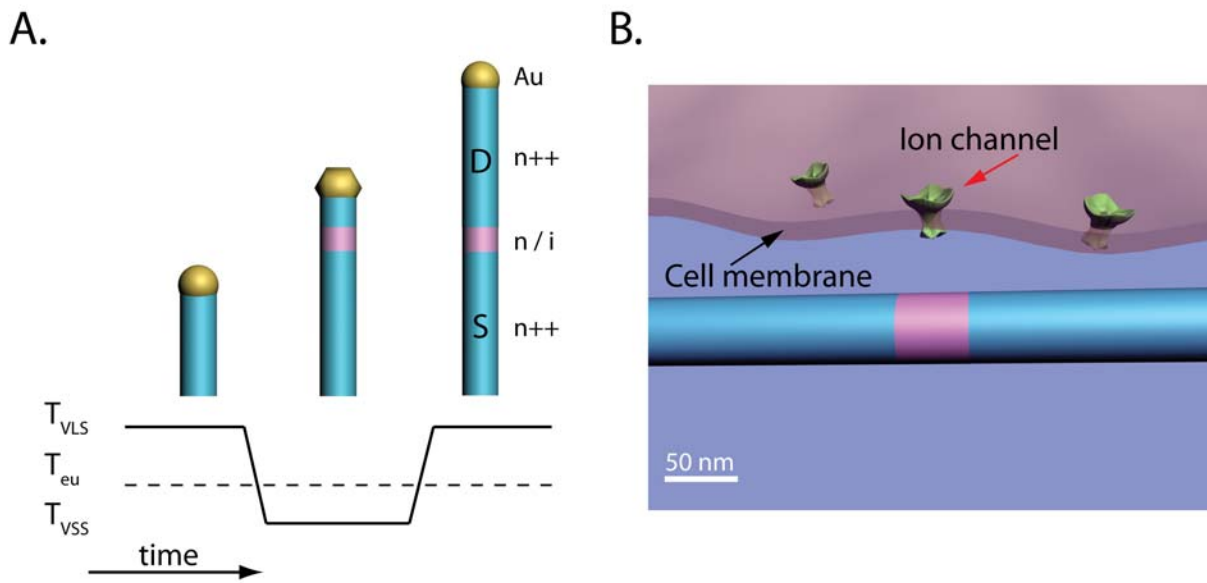
Figure 1. Overview of the synthesis and cellular interfaces of short channel NWFETs. (A) Illustration of Au nanoparticle catalyzed NW growth with well-controlled axial dopant profile introduced during VSS growth. Initially a n^{++} S electrode is synthesized via the VLS mechanism. Subsequently, either n or i active device regions are encoded by VSS growth. Lastly, another VLS phase of growth completes the n^{++} D electrode. (B) Schematic of a short-channel NWFET interfaced with an extracellular region of an electrogenic cell.

The key synthetic parameters for the SiNW short channel devices are characterized in Figure 2. We synthesized NWs with channel lengths of 50, 80, and 150 nm, as exemplified by the SEM images of selectively etched NWs (Figure 2A).[34] Using a calibrated growth rate of ca. 1.0 nm/min (Figure 2B),

4

these three $n^{++}/i/n^{++}$ structures were grown in VSS mode at 340 °C by changing the growth time used for the intrinsic channel.[32] Our growth rates are in good agreement with published data,[27,28] and are ~10-100 times smaller than published VLS growth rates of 100-600 nm/min.[29,30] In addition, phosphorous elemental mapping obtained with an aberration-corrected scanning transmission electron microscope (Cs-STEM) allowed us to characterize the abruptness of the $n^{++}/i/n^{++}$ dopant transition.[33] As shown in Figure 2C, the elemental map and line profile exhibit an abrupt drop in phosphorus (P) counts over a span of ~5 nm within the intrinsic channel of the 80 nm diameter NW. We note that the P counts reading in the "i" region are due in part to the much larger Si signal, which contributes a background to the signal,[35] and possibly surface P-contamination during the final n^{++} segment growth. In contrast, analysis of VLS-grown dopant modulated structures suggest dopant modulation length scale on the order of the NW diameter.[28] These results are in accord with previously synthesized Si/Ge heterostructures using a VSS growth mode[27, 28] and demonstrate the unique capability to encode synthetically sharp, well-defined dopant junctions in the NWs.
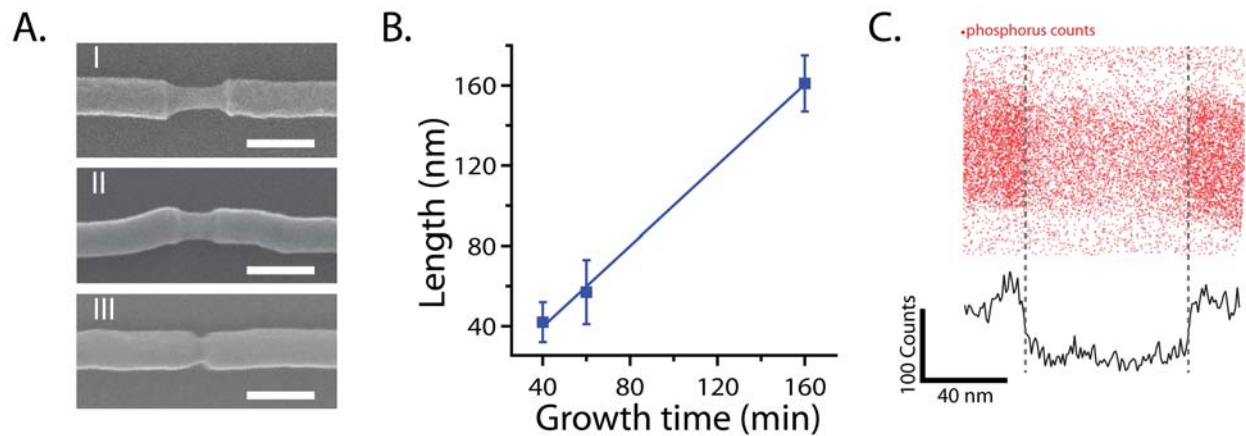
Figure 2. Short channel SiNW synthesis. (A) Short-channel $n^{++}/i/n^{++}$ SiNWs with channel lengths of 150 nm (I), 80 nm (II), and 50 nm (III) using growth times of 160 min, 80 min, and 40 min, respectively, at a VSS growth temperature of 340 °C. Scale bars are 150 nm. The Au catalysts were ~80 nm in diameter and NWs were selectively etched to reveal the active channel. (B) Dependence of the channel length on VSS growth time at 340 °C. Values are average ± SD (calculated for 20 SiNWs per growth time.) (C) EDX elemental mapping of P dopant in an $n^{++}/i/n^{++}$ NW, showing a spatial map of

individual P X-ray counts (top) and line profile of P counts (bottom), generated by radial integration of the P counts shown in the top panel.[33]

The short-channel n^{++}/i or n/n^{++} modulation-doped NWs synthesized in this manner were used to fabricate FET devices as described previously.[4-6, 36] Briefly, S/D contacts to the as synthesized SiNWs were defined by electron beam lithography (EBL) followed by metal deposition, and finally were passivated with SU8 and/or poly(methyl methacrylate) (PMMA).[36] The short-channel NW device performance was characterized by measuring the conductance versus applied water gate potential (Figure 3A). Analysis of the data yields device sensitivities of 13.5, 21.0 and, 6.4 nS/mV for channel lengths of 150 nm, 80 nm, and 50 nm respectively.
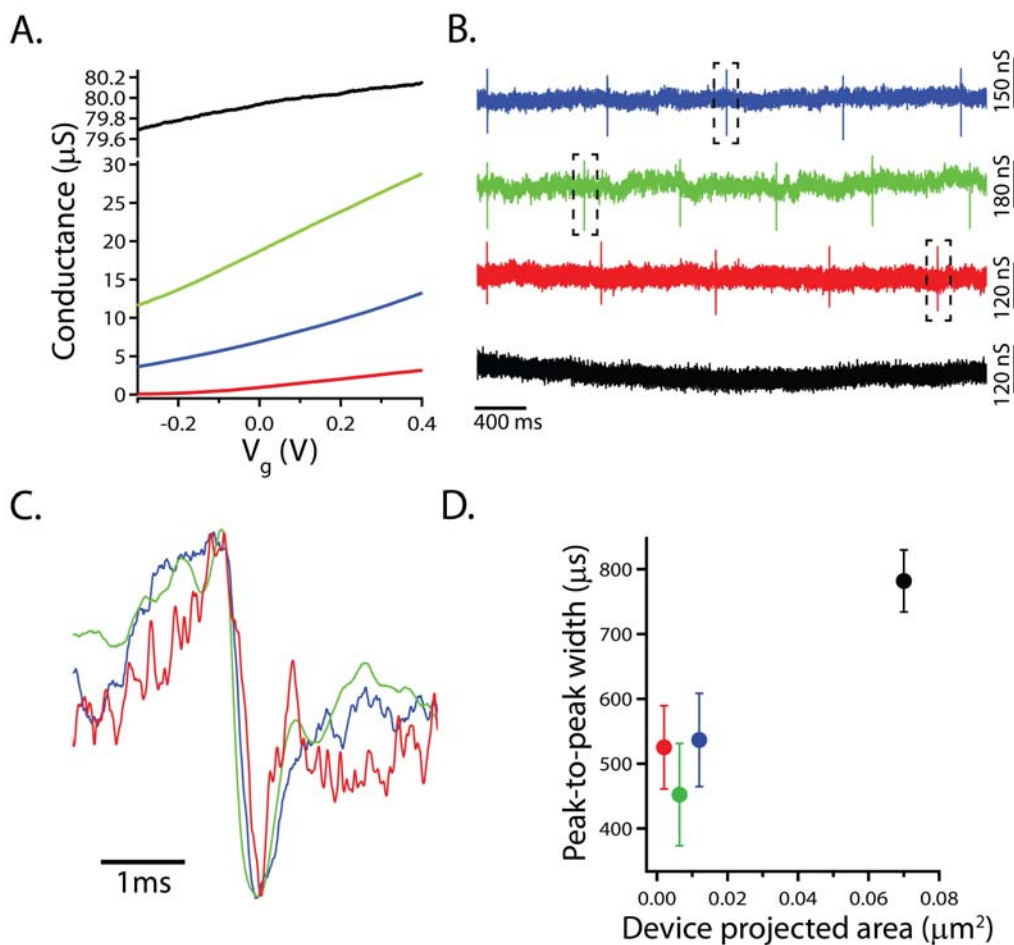
Figure 3. Short channel SiNW FETs interfaced with cardiomyocytes. (A) Conductance of NW FETs as a function of water-gate potential (V_g) for channel lengths of 150 nm (i, blue), 80 nm (i, green), and

50 nm (n, red). Black trace is a control device fabricated on an n^{++} segment without an active channel. (B) Typical recorded signals from beating cardiomyocytes for devices presented in panel A. The n^{++} control (Black trace) was recorded simultaneously with the 80 nm channel length device. For the 50 nm channel length device, a 40 nm diameter NW was used, whereas the other NW devices were 80 nm in diameter. For the 150 and 80 nm channel length devices, $V_g = 0$ V, and for the 50 nm channel length device, $V_g = +0.3$ V. (C) Magnification of single peaks from each of the short-channel devices shown in panel B (black dashed boxes). The amplitudes of the presented expanded peaks are 188, 277 and 160 nS for the 150, 80 and 50 nm channel length devices. (D) Summary of the peak-to-peak widths for the each of the short-channel structures. In addition, a previously published 2.3 μm channel length SiNW device (black) is shown for comparison.[6]

The different short-channel SiNW devices were interfaced with spontaneously beating embryonic chicken cardiomyocytes as previously described.[5, 38, 39] Measurements of conductance versus time yielded regularly spaced peaks with a frequency of 1.1-1.3 Hz (Figure 3B) characteristic of beating cardiomyocyte cells.[5, 6, 8, 9] The recorded signals have calibrated peak-to-peak voltages of 14.4, 12.5, and 25.7 mV and a signal-to-noise ratio (S/N) of 3.1, 2.2, and 2.7 for the 150, 80 and 50 nm channel length devices respectively. These findings show that there is no decrease in the amplitude of the recorded signals with decreasing channel length. To confirm that measured signals arise from the encoded active short-channels (and not from the much longer S/D arms), we also measured the response from a control device fabricated on one of the n^{++} arms. Notably, the control device (Figure 3B black trace) showed no signal, while the short-channel device exhibited periodic peaks characteristic of the beating cell (Figure 3B, green trace).

We have also analyzed the temporal characteristics of individual peaks from the conductance – time data recorded from the different short-channel devices. Representative data (Figure 3C) show that peak-to-peak widths of 520 ± 40, 450 ± 80, and 540 ± 50 μs for 150, 80 and 50 nm channel length devices, respectively. These widths are significantly smaller than the peak-to-peak widths, 750-850 μs,

reported for devices with micron scale active channels[5, 6] (Figure 3D, black circle). Interestingly, the time constants reported for sodium ion channel conduction are ca. 500 µs,[40] which is in good accord with time constants measured from short-channel NW FETs. These results underscore the importance of recording with "point-like" detectors to avoid extrinsic temporal broadening (due to detector averaging), and moreover, suggest that such short-channel NW devices may be capable of measuring ion channel activity on the length and time scale of single ion channel events in future studies.

To further illustrate the capabilities of this bottom-up approach for encoding FET devices we synthesized multiple $n^{++}/i/n^{++}$ channels on an individual SiNWs (Figure S1), and then used EBL to fabricate closely spaced FETs. Three ca. 80 nm short-channel SiNW devices, where the first and second devices are on the same NW and the third device is on a separate NW, interfaced with beating cardiomyocytes are shown in Figure 4A. Conductance versus time data recorded from these three devices (Figure 4B) exhibit clear and correlated extracellular peaks with a ~1 Hz frequency. Quantitative analysis of the time differences between devices is presented in Figure 4C.[6, 41] The signal from device 1 (labeled d1 in Figure 4A) precedes device 2 (d2) and device 3 (d3) because of spatial propagation of the signal from d1 toward d3. Moreover, the signal spreads from d1 to both d2 and d3 with speeds of 0.17 m/s and 0.35 m/s. These propagation speeds are in good agreement with reported propagation speeds values in literature.[42]
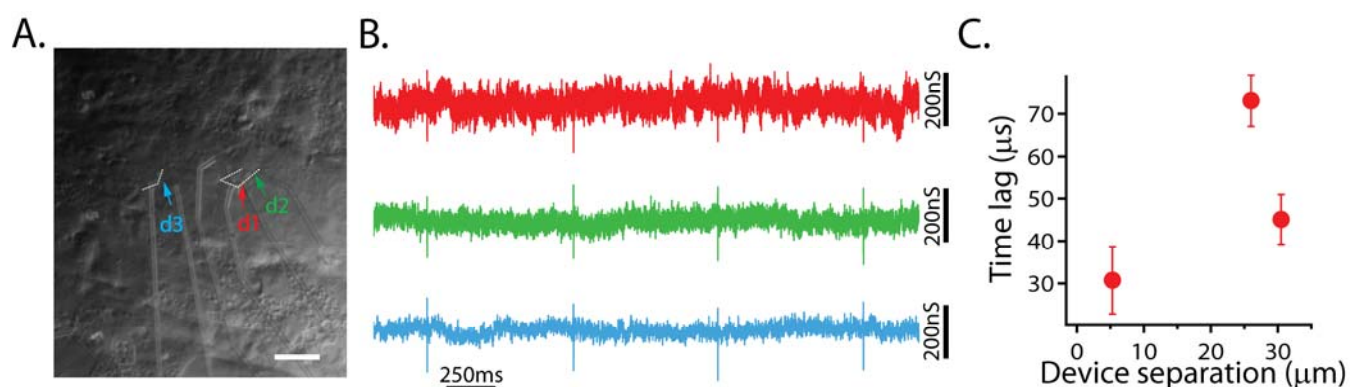
Figure 4. Multiplexed recording with short-channel devices. (A) Optical image of three 80 nm short-channel SiNW devices interfaced with cardiomyocytes. The first and second devices (d1 and d2) are on

the same NW and the third device (d3) is on a separate NW (white dashed lines highlight the NW positions). Scale bar is 15 μm. (B) Representative conductance vs. time signals from d1 (red), d2 (green), and d3 (cyan). (C) Time lag between the three devices as determined by correlation analysis (values are average ± SD, calculated from 58 beating events).[41] The distance between devices was 5.3 μm for d1-d2, 26 μm for d1-d3, and 30.5 μm for d2-d3.

In addition, we have extended our approach of synthetically-encoding devices to separations smaller than 2 μm (Figure 5A and Figure S2). Specifically, three 130 nm short channel devices were interfaced with spontaneously beating cardiomyocytes and used to record the conductance changes as a function of time (Figure 5B). These data show well-defined, correlated extracellular peaks with a ~1 Hz frequency. Data from 375 beating events recorded simultaneously from the three devices were analyzed[41] to determine time differences between pairs of devices. The results (Figure 5C) show time lags of 4.9 and 89 μs for the two devices separated by 1.9 μm (Figure 5A, d1 and d2) and 73 μm (Figure 5A, d1 and d3), respectively. The corresponding signal propagation speeds of 0.4 and 0.8 m/s are in good agreement with published data of signal transduction in cultured cardiomyocytes.[42] Interestingly, the signal propagation across multiple cell junctions, between d3 to d1, showed a larger standard deviation (19 μs) than the case of within a single cell (d2 to d1, 7.6 μs). These results may reflect multiple signal paths over longer distances between cells, although future studies will be required to conclusively illuminate the non-trivial deviations in the distributions, including for example, the dynamic redistribution of density of ion channels over the time course of our recordings.[43]
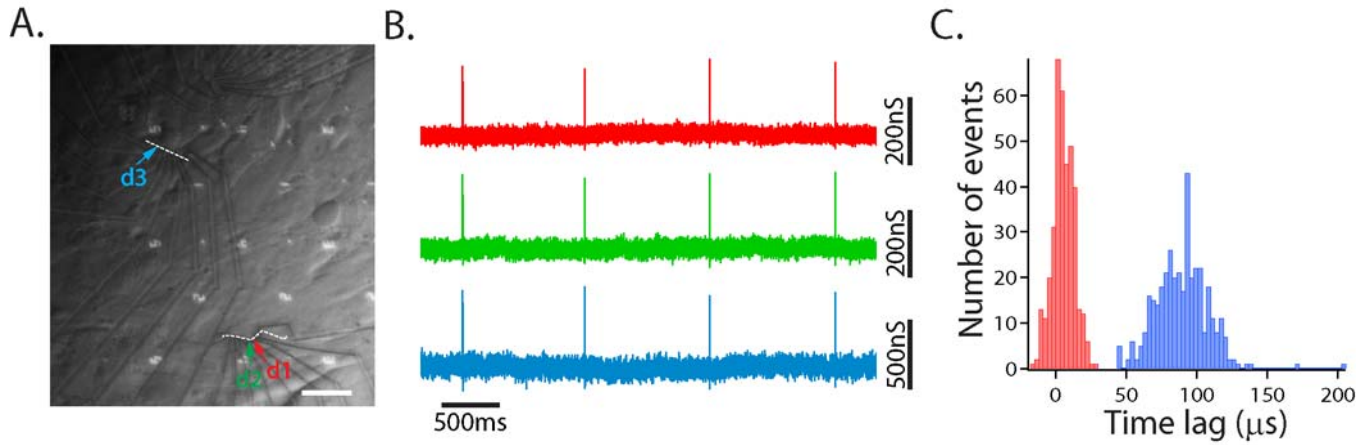
Figure 5. Recording from short-channel SiNW FETs on multiple length scales. . (A) Optical image of cardiomyocytes interfaced with three 130 nm channel length devices (labeled d1, d2, and d3). White dashed lines illustrate the NW position; scale bar is 15 μm. (B) Representative recorded signals from d1 (red), d2 (green), and d3 (blue). (C) Histogram of the time lag between devices d1 and d2 (red; separation distance 1.9 μm) and between devices d1 and d3 (blue; separation distance 73 μm).

In conclusion, we have demonstrated the synthesis of axial dopant modulated ultrashort SiNWs FET devices via the VSS growth method and the use of these devices for recording extracellular field potentials with high spatial resolution. Using the VSS mode, we were able to grow segments as small as 50nm in 40 nm diameter SiNWs. Elemental mapping of phosphorous across the short channel segments revealed a transition length < 5nm, which is an order of magnitude smaller than the VLS transition length. Devices with 150, 80 and 50 nm channel lengths faithfully recorded extracellular field potentials from beating cardiomyocytes, and demonstrated no decrease in the calibrated (voltage) extracellular potentials and S/N with decreasing device size. Temporal analysis of the recorded peaks also revealed distinct differences between these ultrashort devices and longer channel length devices. The peak-to-peak width of the ultrashort devices, ~500 μs, was comparable to the intrinsic time constant for Na^+-ion channels and smaller than longer channel length devices, thus highlighting the potential of these "point-like" detectors for probing ion channel activity. Moreover, the flexibility of the bottom-up synthetic approach allowed us to create multiple ultrashort devices in single SiNWs, allowing us to detect signal

10

propagation at the subcellular level. These findings open up unique opportunities for fundamental, sub-cellular biophysical studies and also make steps toward the limit of building electronic interfaces at close to the molecular level.

11

References.

1.   Zheng, G.; Patolsky, F.; Cui, Y.; Wang, W. U.; Lieber, C. M. *Nat. Biotechnol.* **2005,** *23*, 1294-1301.

2.   Stern, E.; Klemic, J. F.; Routenberg, D. A.; Wyrembak, P. N.; Turner-Evans, D. B.; Hamilton, A. D.; LaVan, D. A.; Fahmy, T. M.; Reed, M. A. *Nature.* **2007,** 445, 519-522.

3.   Patolsky, F.; Zheng, G.; Hayden, O.; Lakedamyali, M.; Zhuang, X.; Lieber, C. M. *P. Natl. Acad. Sci. USA* **2004,** *101*, 14017-14022.

4.   Patolsky, F.; Timko, B. P.; Yu, G.; Fang, Y.; Greytak, A. B.; Zheng, G.; Lieber, C. M., *Science* **2006,** 313*,* 1100-1104.

5.   Cohen-Karni, T.; Timko, B. P.; Weiss, L. E.; Lieber, C. M. *Proc. Natl. Acad. Sci. U S A* **2009**, 106, 7309-7313.

6.   Cohen-Karni, T.; Qing, Q.; Li, Q.; Fang, Y.; Lieber, C. M. *Nano Lett* **2010**, 10, 1098-1102.

7.   Pui, T. S.; Agarwal, A.; Ye, F.; Balasubramanian, N.; Chen, P. *Small* **2009**, 5, 208-212.

8.   Tian, B.; Cohen-Karni, T.; Qing, Q.; Duan, X.; Xie, P.; Lieber, C. M. *Science* **2010**, 329, 830-834.

9.   Duan, X.; Gao, R.; Xie, P.; Cohen-Karni, T.; Qing, Q.; Choe, H.; Tian B.; Jiang, X.; Lieber, C. M. *Nat. Nanotechnol*. **2012**, 7, 174-179.

10.   Timko, B. P.; Cohen-Karni, T.; Yu, G.; Qing, Q.; Tian, B.; Lieber, C. M. *Nano Lett* **2009**, 9, 914-9188.

11.   Qing, Q.; Pal, S. K.; Tian, B.; Duan, X.; Timko, B. P.; Cohen-Karni, T.; Murthy, V. N.; Lieber, C. M. *Proc. Natl. Acad. Sci. U S A* **2010,** 107, 1882-1887.

12.   Halbach, M. D.; Egert, U.; Hescheler, J.; Banach, K. *Cell. Physiol. Biochem.* **2003**, 13, 271-284.

13.   Heer, F.; Hafizovic, S.; Ugniwenko, T.; Frey, U.; Franks, W.; Perriard, E.; Perriard, J.-C.; Blau, A.; Ziegler, C.; Hierlemann, A. *Biosens. Bioelectron.* **2007**, 22, 2546-2553.

14.   Meyer, T.; Boven, K.-H.; Gunther, E.; Fejtl, M. *Drug Safety* **2004**, 27, 763-772.

15.   Yeung, C.-K.; Ingebrandt, S.; Krause, M.; Offenhausser, A.; Knoll, W. *J. Pharmacol. Toxicol. Methods* **2001**, 45, 207-214.

16.   Ingebrandt, S.; Yeung, C.-K.; Krause, M.; Offenhausser, A. *Biosens. Bioelectron.* **2001**, 16, 565-570.

17.   Tian, B.; Xie, P.; Kempa, T. J.; Bell, D. C.; Lieber, C.M. *Nat. Nanotechnol*. **2009**, 4, 824-829.

18.   Stevens, M. M.; George, J. H. *Science* **2005**, 310, 1135-1138.

19.   Sniadecki, N. J.; Desai, R. A.; Ruiz, S. A.; Chen, C. S. *Ann Biomed Eng* **2006**, 34, 59-74.

20. Fadel, T. R.; Steenblock, E. R.; Stern, E.; Li, N.; Wang, X.; Haller, G. L.; Pfefferle, L. D.; Fahmy, T. M. *Nano Lett* **2008**, 8, 2070-2076.

21. Park, J.; Bauer, S.; von der Mark, K.; Schmuki, P. *Nano Lett* **2007**, 7, 1686-1691.

22. Mooney, E.; Dockery, P.; Greiser, U.; Murphy, M.; Barron, V. *Nano Lett* **2008**, 8, 2137-2143.

23. Cellot, G.; Cilia, E.; Cipollone, S.; Rancic, V.; Sucapane, A.; Giordani, S.; Gambazzi, L.; Markram, H.; Grandolfo, M.; Scaini, D.; Gelain, F.; Casalis, L.; Prato, M.; Giugliano, M.; Ballerini, L. *Nat Nanotechnol* **2009**, 4, 126-133.

24. Arnold, M.; Cavalcanti-Adam, E. A.; Glass, R.; Blummel, J.; Eck, W.; Kantlehner, M.; Kessler, H.; Spatz, J. P. *Chemphyschem* **2004**, 5, 383-388.

25. Graeter, S. V.; Huang, J. H.; Perschmann, N.; Lopez-Garcia, M.; Kessler, H.; Ding, J. D.; Spatz, J. P. *Nano Lett* **2007**, 7, 1413-1418.

26. Hu, Y.; Xiang, J.; Liang, G.; Yan , H.; Lieber, C.M. *Nano Lett.* **2008**, 8, 925-930.

27. Kodambaka, S.; Tersoff, J.; Reuter, M. C.; Ross, F. M. *Science* **2007**, 316, 729-732.

28. Wen, C. Y.; Reuter, M. C.; Bruley, J.; Tersoff, J.; Kodambaka, S.; Stach, E. A.; Ross, F. M. *Science* **2009**, 326, 1247-1250.

29. Schmidt, V.; Wittemann, J. V.; Gösele, U. *Chem Rev* **2010**, 110, 361-388.

30. Yang, C. W.; Zhong, Z.; Lieber, C. M. *Science* **2005**, 310, 1304-1307.

31. Clark, T. E.; Nimmatoori, P.; Lwe, K. −K., Pan, L.; Redwing, J. M.; Dickey, E. C. *Nano Lett* **2008**, 8, 1246-1252.

32. An example of a typical growth conditions. n^{++} arm - 1.25 sccm SiH_4, 14.4 sccm PH_3, 100 sccm H_2, T= 405°C, pressure = 60 torr. VSS mode grown lightly doped (n) device region: 2.5sccm SiH_4, 0.44 sccm PH_3, 100 sccm H_2, T= 340°C, pressure = 100 torr. VSS mode grown intrinsic (i) device regions: 1.25sccm SiH_4, 100 sccm H_2, T= 340°C, pressure = 100 torr.

33. For phosphorous dopant mapping by EDS, $n^{++}/i/n^{++}$ NWs were synthesized as described above. The SiNWs were dispersed on ultra-thin carbon film TEM copper grid and were loaded in the aberration corrected scanning TEM (cs-STEM, Libra 200 MC, Carl Zeiss NTS), which is equipped with twin EDS detectors and drift correction. The EDS elemental map for P were stored at 512×400 resolution and acquired over 4 hours using a 500 ms pixel dwell time and 1.2 nm spot size.

34. We used KOH selective etching in order to analyze the transition between n^{++} to intrinsic sections. 10gr of KOH (Sigma-Aldrich Inc.) were dissolved in 88mL DI H_2O and 37mL isopropanol. Substrates with dispersed NWs were dipped in the solution for 3-8sec at 50°C-60°C. The substrates were rinsed with DI H_2O, followed with isopropanol rinse and N2 bow dried. Following the etching the substrates were imaged using SEM (5-10keV) and the images were analyzed to quantify the transition length.

35. Kempa, T. J.; Cahoon, J. F.; Kim, A. −K.; Day, R. W.; Bell, D. C.; Park, H. −G.; Lieber, C. M. *Proc. Natl. Acad. Sci. USA* **2012** 109, 1409-1412.

36. The short channel device region was located by either a kink in the SiNW induced due to the temperature change between VLS and VSS or by using the Au nanoparticle as a reference point for the interconnects design (as can be seen in Figure S1). Following this step, short channel SiNW devices were fabricated by e-beam lithography (EBL) (30keV), metalized by thermal evaporation of 5nm Cr/100nm Au/20nm Cr. Last, the substrate is coated with 300 nm poly(methyl methacrylate) (150 nm PMMA 495 C2, 150 nm PMMA 950 C2, Microchem Corp.) as a passivation layer, and 4μm X 9μm windows were opened only at the SiNW devices by another EBL step (30keV). We note that in some cases we used an additional SU8 2000.5 (Microchem Corp.) as a passivation layer for the device interconnects.

37. The S/N was calculated as follows. The noise was evaluated for each of the presented traces by first calculating the standard deviation (SD) of the base line and then multiplying it by a factor of 6 to get the peak-to-peak noise level. Following this we divided the peak-to-peak amplitudes for each of the traces by the baseline noise. For example, the noise level for the devices mentioned in Figure 3B is 63, 122, 60 nS for the 150, 80 and 50 nm channel length respectively. The corresponding amplitudes of the recorded signals are 194, 264, and 164 nS for 150, 80 and 50 nm channel length respectively. Resulting with S/N of 3.1, 2.2, 2.7 respectively.

38. White Leghorn chick embryos (Charles River Labs) were maintained in a humidified incubator (Carolina Biological Supply Company) at 37.5°C, and hearts were isolated from embryos at E10 - E15 stage. Isolated hearts were immediately transferred to a phosphate buffer solution maintained at 37.5°C. The hearts were minced and then digested in collagenase II (Gibco, Inc.) until all the heart tissue disintegrated into cells. The cell suspension was then centrifuged and the supernatant was discarded, the cell pellet was resuspended in 10% FBS DMEM medium and was incubated for 1 h in a 75 mL flask to clean the cell culture as much as possible from fibroblasts. After 1 h the cell suspension was then collected, cells were

counted using a standard hemacytometer and were seeded on PDMS thin sections modified with Fibronectin (BD, Biosciences Inc) with concentrations varying between 2.5×10^5 cells/mL to 2×10^6 cells/mL. The medium was exchanged with N2 (Invitrogen, Inc.) supplemented DMEM:F12 (ATCC, Inc.) medium after 24 h and then every other day. Cells spontaneously contracted after 1-2 days in culture.

39.   All studies were carried at 37.5°C using Tyrode solution (Sigma-Aldrich Inc.). An Ag/AgCl wire was used as a reference electrode. The short channel SiNW-FET conductance was measured with DC bias set to 50 mV using a battery source. The drain current was amplified with a variable gain amplifier (1211 current preamplifier, DL Instruments, Inc.) and filtered using a low pass of 0-6kHz filter (CyberAmp 380, Molecular Devices). The output signal was recorded at an acquisition rate of 50-4000 kHz using a multichannel A/D converter (Digidata 1440A, Molecular Devices) interfaced with a PC running pClamp 10.1 electrophysiology software (Molecular Devices). Post-analysis was completed in Igor Pro (Wavemetrics).

40.   Hille, B. *Ion channels of excitable membranes*. 2001, 3rd edition, Sinauer.

41.   Timing delays were calculated using a standard cross-correlation technique. Briefly, each trace in Figure 3B was loaded in its entirety into Matlab (The Mathworks, Inc.) as a single-column matrix. Each matrix (X_i) was normalized by $X_{i,norm} = (X_i - \text{mean}(X_i)) / \text{std}((X_i - \text{mean}(X_i))$, where mean and std are standard Matlab functions for calculating mean and standard deviation, respectively. Unbiased cross-correlation analysis was performed on pairs of normalized matrices (X_1, X_2) using the built-in xcorr function. The cross-correlation function ($X_1 \star X_2$) is a curve with maximum shifted slightly from zero; this shift represents the time-offset between the paired input matrices.

42.   Fast, V.G.; Kleber, A. G. *Circ. Res.* **1994**, 75, 591-595.

43.   Dubach, J. M.; Das, S.; Rozenzweig, A.; Clark, H. A. *Proc Natl Acad Sci U S A* **2009**, 106, 16145-16150.

TOC Graphic
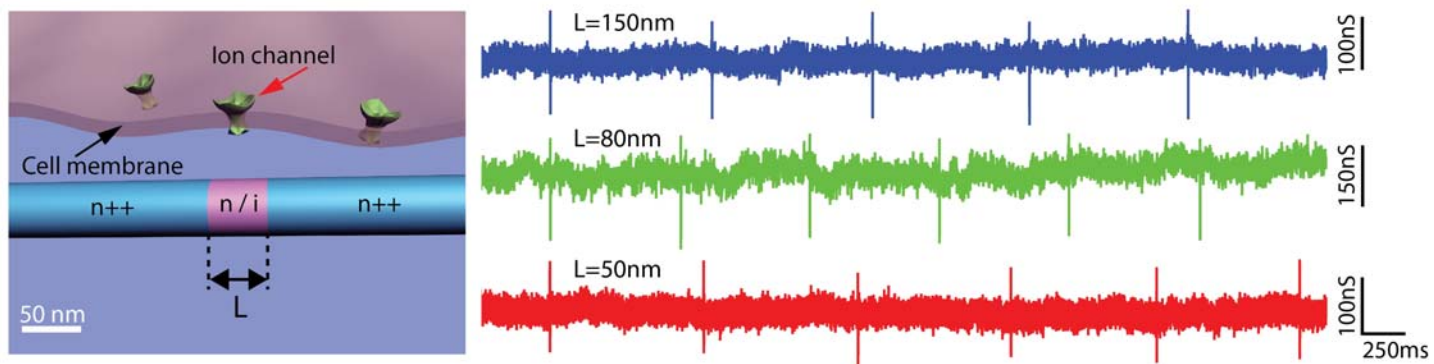
Synthetically-encoded ultrashort-channel nanowire transistors for fast, point-like cellular signal detection

Tzahi Cohen-Karni[†], Didier Casanova[‡], James F. Cahoon[‡], Quan Qing [‡], David C. Bell[†,#], Charles M. Lieber*[†,‡]
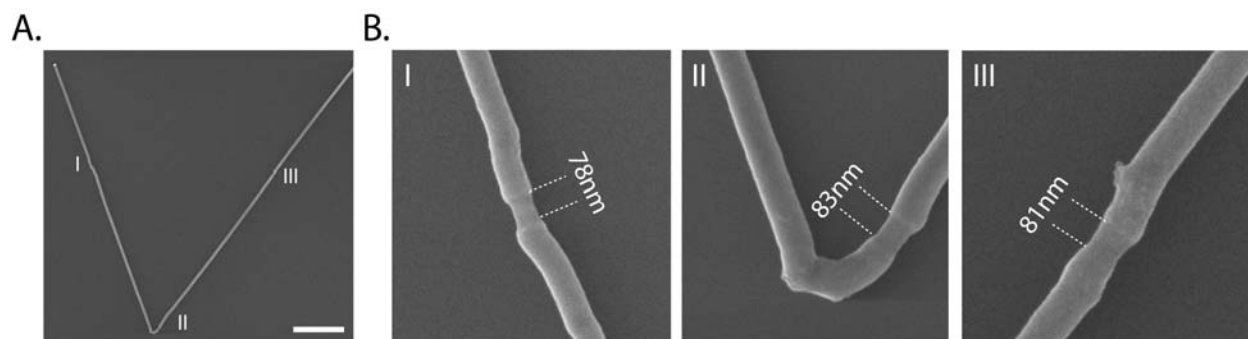
[†]School of Engineering and Applied Science, Harvard University, Cambridge, Massachusetts 02138

[‡]Department of Chemistry and Chemical Biology, Harvard University, Cambridge, Massachusetts 02138

[#]Center for Nanoscale Systems, Harvard University, Cambridge, Massachusetts 02138

This file includes:

  Supplementary Figures S1 and S2

Figure S1. Multiple short channel NWs synthesized on a single Si NW. A. SEM image of a representative 80 nm Si NW with three 80 nm channel length devices. Scale bar is 1.5 μm. B. An expanded view of the short channel segments marked as I, II and III. Synthesized SiNWs were dispersed from isopropanol solutions onto the nitride surface of $Si/SiO_2/Si_3N_4$ substrates (NOVA Electronic Materials Inc.), then KOH selective etching was used to highlight the transition between n^{++} to intrinsic sections. 10gr of KOH (Sigma-Aldrich Inc.) were dissolved in 88mL DI H_2O and 37mL isopropanol. Substrates with dispersed NWs were dipped in the solution for 3-8sec at 50°C-60°C. The substrates were rinsed with DI H_2O, followed with isopropanol rinse and dried in a N_2 stream.
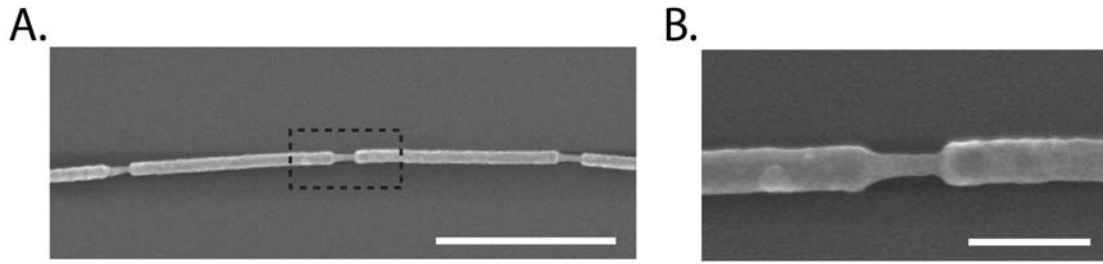
Figure S2. Short channel Si NW FETs designed for recording on multiple length scales. A. SEM image of an 80 nm diameter NW encoded with 130 nm channel lengths that are separated by 1.1 μm; scale bar is 1μm. B. An expanded view of the segment marked with a black dashed box; scale bar is 200 nm. Synthesized SiNWs were dispersed from isopropanol solutions onto the nitride surface of $Si/SiO_2/Si_3N_4$ substrates (NOVA Electronic Materials Inc.), then KOH selective etching was used to highlight the transition between n^{++} to intrinsic sections. 10gr of KOH (Sigma-Aldrich Inc.) were dissolved in 88mL DI H_2O and 37mL isopropanol. Substrates with dispersed NWs were dipped in the solution for 3-8sec at 50°C-60°C. The substrates were rinsed with DI H_2O, followed with isopropanol rinse and dried in a N_2 stream.